J Neurophysiol
88: 2430–2444, 2002; 10.1152/jn.00839.2001.

A Biophysical Model of Nonlinear Dynamics Underlying Plateau Potentials and Calcium Spikes in Purkinje Cell Dendrites

STÉPHANE GENET AND BRUNO DELORD
Institute National de la Santé et de la Recherche Médicale U.483, Université Pierre et Marie Curie, Boîte 23, 75252 Paris Cedex 05, France

Received 15 October 2001; accepted in final form 24 July 2002

Genet, Stéphane and Bruno Delord. A biophysical model of nonlinear dynamics underlying plateau potentials and calcium spikes in Purkinje cell dendrites. *J Neurophysiol* 88: 2430–2444, 2002; 10.1152/jn.00839.2001. Computational capabilities of Purkinje cells (PCs) are central to the cerebellum function. Information originating from the whole nervous system converges on their dendrites, and their axon is the sole output of the cerebellar cortex. PC dendrites respond to weak synaptic activation with long-lasting, low-amplitude plateau potentials, but stronger synaptic activation can generate fast, large amplitude calcium spikes. Pharmacological data have suggested the involvement of only the P-type of Ca channels in both of these electric responses. However, the mechanism allowing this Ca current to underlie responses with such different dynamics is still unclear. This mechanism was explored by constraining a biophysical model with electrophysiological, Ca-imaging, and single ion channel data. A model is presented here incorporating a simplified description of $[Ca]_i$ regulation and three ionic currents: *1*) the P-type Ca current, *2*) a delayed-rectifier K current, and *3*) a generic class of K channels activating sharply in the sub-threshold voltage range. This model sustains fast spikes and long-lasting plateaus terminating spontaneously with recovery of the resting potential. Small depolarizing, tonic inputs turn plateaus into a stable membrane state and endow the dendrite with bistability properties. With larger tonic inputs, the plateau remains the unique equilibrium state, showing long traces of transient inhibitory inputs that are called "valley potentials" because their dynamics mirrors that of inverted, finite-duration plateaus. Analyzing the slow subsystem obtained by assuming instantaneous activation of the delayed-rectifier reveals that the time course of plateaus and valleys is controlled by the slow $[Ca]_i$ dynamics, which arises from the high Ca-buffering capacity of PCs. A bifurcation analysis shows that tonic currents modulate sub-threshold dynamics by displacing the resting state along a hysteresis region edged by two saddle-node bifurcations; these bifurcations mark transitions from finite-duration plateaus to bistability and from bistability to valley potentials, respectively. This low-dimensionality model may be introduced into large-scale models to explore the role of PC dendrite computations in the functional capabilities of the cerebellum.

INTRODUCTION

The cerebellum is one of the principal regions of the brain implicated in adaptive control of movements (Ito 1984). The way this nervous structure operates during acquisition of motor skills remains, however, a matter of debate. Central to this issue are computational capabilities of Purkinje cells (PCs), because axons from these large neurons constitute the sole output of the cerebellar cortex. Information originating from nearly the entire nervous system converges onto PC dendrites in the form of two excitatory inputs—hundreds of thousands parallel fibers (PFs) contact the distal spiny dendrites while a single climbing fiber (CF) establishes a distributed, powerful synapse on the proximal smooth dendrites. The two inputs interact through the PC dendritic tree, which is endowed with highly nonlinear membrane properties (Llinas and Sugimori 1992).

Stimulation of PC dendrites can result in two very different types of nonlinear calcium-dependent responses: weak stimulation causes low-amplitude plateau potentials, which can last up to several hundred milliseconds until the resting potential is spontaneously restored, and stronger stimulation can generate fast, large amplitude Ca spikes (Llinas and Sugimori 1980b). In vivo, Ca spikes underlie the so-called "complex spike" evoked by activation of the CF (Eccles et al. 1966), which results in a generalized $[Ca]_i$ increase in the dendrites. Plateau potentials are low-amplitude (approximately 15 mV) depolarizations from resting potential. They exhibit a threshold behavior and display variable duration ranging from 100 ms to several seconds (Ekerot and Oscarsson 1981; Llinas and Sugimori 1980b, 1992). Plateaus putatively participate in dendritic computations and synaptic plasticity, but these roles could not be explored thoroughly due to an uncertain mechanism underlying these electric signals. Several models have attempted to understand this mechanism, like the large-scale, multi-compartmental PC model of De Schutter and Bower (1994). This model sustains plateaus, but these are unconditionally stable and do not account for spontaneous reset of experimental plateaus. Miyasho et al. (2001) have recently proposed a modified version of this model, which produces finite-duration plateaus, but these are not all-or-none. Such discrepancies with experimental plateaus are difficult to interpret, due to the complexity of models incorporating numerous ion channel types. Yuen et al. (1995) have adopted an opposing viewpoint by building a simple model that sustains spikes and plateaus. However, their model displays plateaus at unrealistic depolarized potentials that do not spontaneously reset. Moreover, their model predicts transition from spiking to plateaus with increasing stimuli, whereas Llinas and Sugimori (1980b) have observed the op-

Address for reprint requests: Institute National de la Santé et de la Recherche Médicale U.483, Université Pierre et Marie Curie, Boîte 23, 75252 Paris Cedex 05, France (E-mail: stephane.genet@snv.jussieu.fr).

The costs of publication of this article were defrayed in part by the payment of page charges. The article must therefore be hereby marked "*advertisement*" in accordance with 18 U.S.C. Section 1734 solely to indicate this fact.

posite transition in intracellular recordings. Thus either simplistic or detailed descriptions of membrane properties have failed to interpret the dual electroresponsiveness of PC dendrites.

The objective of this study was to investigate the minimal biophysical properties required to produce the dual electroresponsiveness of PC dendrites. The strategy was to build up a computationally tractable model that may subsequently be introduced into network models of the cerebellum. For the model presented in this paper to be conclusive, several constraints were imposed: *1*) the model had to reproduce characteristic features of plateaus, including shape, amplitude, duration, and the threshold behavior evidenced by Llinas and Sugimori (1980b); *2*) the model also reproduced landmark electrophysiological properties such as passive membrane properties and Ca spiking; and *3*) the model was based on a careful use of available ion channel data to avoid interpretations based on peculiar solutions of poorly constrained models.

Here we present a biophysical model that shows that plateau potentials and calcium spikes can both be generated by the same underlying currents: the P-type Ca current, a delayed rectifier K current and a sub-threshold, generic K current that lumps together the set of low-voltage activated K currents described in PCs (Gruol et al. 1989, 1991; Jacquin and Gruol 1999; Midtgaard 1995; Midtgaard et al. 1993; Wang et al. 1991). The plateaus of the model give a correct quantitative fit for experimental plateaus. Besides, a yet unobserved form of inverted plateau, or "valley potential," emerges as a natural property of the saddle-node bifurcation underlying the existence of plateaus. A robustness analysis proves that the results are not dependent on the particular set of parameters used in the simulations. Availability of this reliable, simplified model sets the stage for future studies on the role of PC dendrites computations in information processing in the cerebellum.

DENDRITIC MODEL

Electric properties of the membrane

The present study examines an isopotential, single-compartment model of a dendrite with radius R_d (centimeters) (Fig. 1). In mature PCs, P-type Ca channels sustain more than 90% of dendritic Ca currents (Kaneda et al. 1990; Usowicz et al. 1992), and the dendritic membrane is devoid of voltage-dependent Na channels (Llinas and Sugimori 1992; Stuart and Haüsser 1994). The model, therefore incorporated the P-type Ca conductance as the unique voltage-dependent inward conductance. The situation is less clear regarding outward conductances. In 1989, Gähwiler and Llano identified two types of K conductances with single-channel recordings from PCs. One had properties reminiscent of the delayed-rectifier, while the other was suggested to correspond to a large-conductance, Ca-dependent K channel (or "BK-type" channel, see Hille 1992). Gruol and collaborators later extended these findings. On the one hand, they correlated activity of the delayed rectifier to the repolarization phase of spikes (Gruol et al. 1991); we therefore incorporated a delayed rectifier potassium conductance (K_{dr}) in our model, which was adapted from the model of Yuen et al. (1995). On the other hand, Jacquin and Gruol (1999) showed that the Ca-dependent K conductance presents significant sub-threshold voltage activation at Ca concentrations as low as 100 nM. Gruol et al. (1991) found four more K channel types that still have not been clearly identified. However, Midtgaard (1995) has reviewed experimental evidence suggesting that several sub-threshold, inactivating conductances may participate in synaptic integration in PCs dendrites (Midtgaard 1995; Midtgaard et al. 1993). Following the same direction, Wang et al. (1991) characterized a fast-inactivating ($\tau < 100$ ms) A-type conductance, but the existence of a conductance inactivating on the second time scale was suggested by Midtgaard (1995). All in all, a precise identification of sub-threshold K conductances is still lacking. However, as they all activate in a critical voltage range between -50 and -30 mV, which is more negative than the activation threshold for the K_{dr} channel (Gruol et al. 1991), we have lumped these currents into a generic I_{Ksub}, embedded with voltage activation at sub-threshold potentials.

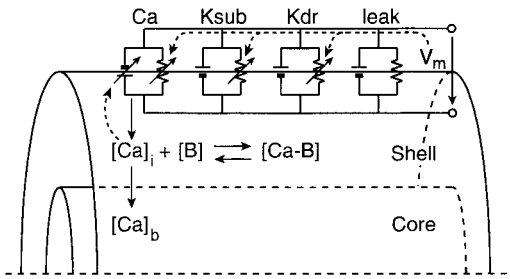

FIG. 1. Membrane of the dendritic model is comprised of a constant leakage conductance and 3 voltage-dependent conductances: g_{Ca} is a high-threshold, P-type Ca conductance, g_{Kdr} is a classical delayed-rectifier, and g_{Ksub} is a low-threshold K conductance. As Ca channels open, Ca^{2+} ions entering the dendrite distribute uniformly into a shell of cytoplasm, inside which they combine with an endogenous buffer and are pumped into an inner core; the Ca concentration in the core is kept at a low basal value, $[Ca]_b$. $[Ca]_i$ changes in the cytoplasm modify the value of the electromotive force on Ca^{2+} ions across the membrane.

In the present model, dynamics of the membrane potential, V (in millivolts), obeyed the differential equation

$$C\frac{dV}{dt} = -(I_{Ca} + I_{Kdr} + I_{Ksub} + I_{Leak}) + I_{dc} + I_{\phi} \quad (1)$$

where C (μFcm^{-2}) stands for the specific membrane capacitance; I_{leak} is a leakage current, and I_{Φ} and I_{dc}, respectively, denote phasic and tonic currents injected into the model. The different ionic currents (expressed as $nAcm^{-2}$ densities) were derived from Ohm's law according to the Hodgkin-Huxley (HH) formalism

$$I_{Ca} = g_{Ca}s(V - E_{Ca}) \quad (2a)$$

$$I_{Ksub} = g_{Ksub}u^3(V - E_{Ksub}) \quad (2b)$$

$$I_{Kdr} = g_{Kdr}n^4(V - E_{Kdr}) \quad (2c)$$

$$I_{Leak} = g_{Leak}(V - E_{Leak}) \quad (2d)$$

where E_{Ca}, E_{Ksub}, and E_{Kdr} represent Nernst potentials and g_{Ca}, g_{Ksub}, and g_{Kdr} correspond to maximum channel conductance (μScm^{-2}). In the HH formulation, actual conductance are given by the product of these maximum conductance by voltage- (and possibly $[Ca]_i$-) dependent gating variables, which are dimensionless functions defined on the range [0,1]; s stands for the activation variable of the Ca current and u and n for that of the sub-threshold and delayed-rectifier K currents, respectively. These variables obey the general differential equation

$$\frac{dp}{dt} = (p_\infty(V) - p)/\tau_p(V), \quad p = s, u, n \tag{3}$$

where $\tau_p(V)$ is the relaxation time and $p_\infty(V)$ is the equilibrium value of variable p. As P-type channels activate very fast (Regan 1991), we equated s to its equilibrium value s_∞ in *Eq. 2a*. The same assumption was made for I_{Ksub}, whose activation variable u was described by its equilibrium value u_∞. As spiking requires delayed activation of I_{Ca} and I_{Kdr}, the latter current was assumed to activate with a classical, bell-shaped time constant (Hille 1992)

$$\tau_n(V) = \tau_{n0} + \tau_{n1}/(\exp[(V - V_{\tau n})/k_{\tau n}] + c_{\tau n}/\exp[(V - V_{\tau n})/k_{\tau n}])^{-1} \tag{4}$$

The different parameters appearing in this equation have the following units: τ_{n0} and τ_{n1} are in milliseconds, $c_{\tau n}$ is dimensionless, and $V_{\tau n}$ and $k_{\tau n}$ are in millivolts. Full HH description of membrane currents implicated unnecessarily complicated calculations given the experimental uncertainty on rates of (in)activation of these currents. Steady-state values of voltage-sensitive gates were therefore described with Boltzmann functions

$$p_\infty(V) = (1 + \exp[-(V - V_p)/k_p])^{-1} \tag{5}$$

where V_p (in millivolts) and k_p (in millivolts), respectively, stand for the half-activation potential and activation slope of gating variable p. *Equation 2b* deserves special comments. The body of results presented in this paper was obtained with the generic I_{Ksub} described in *Eq. 2b*. However, the various subthreshold conductances lumped in I_{Ksub} must display some heterogeneity in their activation function. We therefore investigated the robustness of the results to variations in g_{Ksub}, V_u, and k_u. Moreover, some of these conductances exhibit Ca-dependence or inactivation as noted above, which led to the possibility that these properties may challenge conclusions derived from the crude description of I_{Ksub}. We therefore considered alternative schemes introducing these properties. To model A-type conductances (Midtgaard 1995; Wang et al. 1991), simulations were run with I_{Ksub} multiplied by an inactivation variable h, whose dynamics obeyed *Eq. 3*, with the time constant (τ_h) left as a freely adjustable parameter. Other simulations were run with activation of g_{Ksub} depending on $[Ca]_i$ to mimic the BK-type K conductance of Gruol et al. (1991). Sensitivity of BK channels to $[Ca]_i$ consists in a shift of their activation range toward more negative potentials with increasing concentrations of the cation (Hille 1992). Jacquin and Gruol's (1999) data on this shift were fitted by the following equation for the half-activation potential of g_{Ksub}

$$V_\mu(\mathrm{Ca}) = 3 \times 10^2 \exp[-([Ca]_i - K_{dCa})/k_{Ca}]/ (1 + \exp[-([Ca]_i - K_{dCa})/k_{Ca}]) - 10^2 \tag{6}$$

which was substituted into *Eq. 5*.

Internal dendritic calcium regulation

Ca-imaging techniques have revealed large $[Ca]_i$ increases in PC dendrites on activation of their excitatory synapses (Callaway et al. 1995; Miyakawa et al. 1992). These concentration changes modify the Nernst potential (mV) of Ca ions

$$E_{Ca} = \frac{RT}{2F} \ln \frac{[Ca]_o}{[Ca]_i} \tag{7}$$

and the magnitude of Ca currents at a given membrane potential (see *Eq. 2a*); R is the gas constant ($JK^{-1}M^{-1}$), T is the absolute temperature (K), and F is the Faraday constant (CM^{-1}). Limited knowledge of the numerous processes involved in $[Ca]_i$ regulation hindered elaboration of a faithful model of this concentration effect. A number of simplifying assumptions were thus made to derive a simple model of $[Ca]_i$ dynamics coherent with the low resting Ca level in neurons and calcium imaging data. First, lateral diffusion of Ca along the dendrite was neglected as the cation diffuses slowly within neurons (Hille 1992). Second, Terasaki et al. (1994) have shown that the endoplasmic reticulum extends in PCs from the soma up to the very tip of dendrites and even inside spines. Ca entering the dendrites is therefore compelled to distribute within a thin shell of cytoplasm beneath the membrane; its thickness was taken as $\delta = 0.3$ μm. We assumed that Ca can exchange between this shell and the inner dendritic core (Fig. 1); $[Ca]_i$ in the core was fixed to value $[Ca]_b$. This naive representation was aimed at providing a simple formalism for the complicated processes of calcium diffusion and pumping into the ER. Besides, PCs have a high Ca-buffering capacity (Fierro and Llano 1996), which must markedly slow down $[Ca]_i$ dynamics, according to the modeling work of Sala and Hernandez-Cruz (1990). In consequence, we have introduced, in the model, an immobile calcium buffer with fixed concentration $[B]_T$. With these assumptions, the balance equation of Ca in the sub-membrane shell can be written

$$\frac{d[Ca]_i}{dt} = \Pi - \frac{10^{-9} R_d I_{Ca}}{F\delta(2R_d - \delta)} - \frac{2k(R_d - \delta)([Ca]_i - [Ca]_b)}{\delta(2R_d - \delta)} \tag{8}$$

The rightmost term in *Eq. 8* corresponds to the Ca exchange between the cytoplasm and the inner core of the dendrite, the calcium concentration being kept constant at value $[Ca]_b$ in the latter compartment; this process has a time constant $\delta(2R_d - \delta)/[2k(R_d - \delta)]$, where k corresponds to a one-dimensional diffusion constant (cms^{-1}). Π (μMs^{-1}) denotes a sink term accounting for the binding of Ca to the buffer. This process was described by a first order reaction

$$\mathrm{Ca} + \mathrm{B} \underset{k_2}{\overset{k_1}{\rightleftharpoons}} \mathrm{Ca{-}B}$$

with dissociation constant $K_d = k_2/k_1$ (μM). Introducing the total buffer concentration $[B]_T = [Ca\text{-}B] + [B]$ (μM), the sink term is written

$$\Pi = \frac{d[B]}{dt} = k_1[K_d([B]_T - [B]) - [Ca]_i[B]] \tag{9}$$

Binding of Ca ions to the buffer was assumed to be fast with respect to the overall evolution time of $[Ca]_i$. The free buffer concentration, [B], could therefore be equated to its equilibrium value at each point in time

$$[B] = \frac{[B]_T}{1 + [Ca]_i/K_d} \tag{10}$$

Applying the chain rule of differentiation to *Eq. 10* leads to

$$\Pi = \frac{d[B]}{d[Ca]_i}\frac{d[Ca]_i}{dt} = -\frac{[B]_T/K_d}{(1 + [Ca]_i/K_d)^2}\frac{d[Ca]_i}{dt} \tag{11}$$

This expression was substituted for Ð into *Eq. 8* to obtain

$$\frac{d[\mathrm{Ca}]_i}{dt} = -\left[1 + \frac{[\mathrm{B}]_T/K_d}{(1 + [\mathrm{Ca}]_i/K_d)^2}\right]^{-1} \times \left[\frac{10^{-9}R_d}{\delta(2R_d - \delta)F} I_{Ca} + \frac{2k(R_d - \delta)}{\delta(2R_d - \delta)}([\mathrm{Ca}]_i - [\mathrm{Ca}]_b)\right] \quad (12)$$

Basic parametric values were as follows: $C = 1\ \mu\mathrm{Fcm}^{-2}$, $T = 298$ K, $F = 96,500\ \mathrm{Cmol}^{-1}$, $R = 8.32\ \mathrm{JK}^{-1}\mathrm{mol}^{-1}$, $R_d = 5 \times 10^{-5}$ cm, $[\mathrm{B}]_T = 150\ \mu$M, $K_d = 1\ \mu$M, $[\mathrm{Ca}]_b = 50$ nM, $[\mathrm{Ca}]_o = 1.1$ mM, $\delta = 3 \times 10^{-5}$ cm, $k = 0.01\ \mathrm{cms}^{-1}$, $g_{leak} = 20\ \mu\mathrm{Scm}^{-2}$, $g_{Ca} = 600\ \mu\mathrm{Scm}^{-2}$, $g_{Ksub} = 30\ \mu\mathrm{Scm}^{-2}$, $g_{Kdr} = 4{,}200\ \mu\mathrm{Scm}^{-2}$, $E_{Leak} = -60$ mV, $E_{Ksub} = -95$ mV, $E_{Kdr} = -95$ mV, $V_s = -22$ mV, $V_u = -44.5$ mV, $V_n = -25$ mV, $k_s = 4.53$ mV, $k_u = 3$ mV, $k_n = 11.5$ mV, $\tau_{n0} = 0.2$ ms, $\tau_{n1} = 4.15$ ms, $c_{\tau n} = 0.6$, $k_{\tau n} = 17$ mV, $V_{\tau n} = -22.5$ mV; g_{Ksub} inactivation: $V_h = -50$ mV, $k_h = 8$ mV; Ca-dependence of g_{Ksub}: $K_{dCa} = 10$ nM, $k_{Ca} = 200$ nM.

Analytical and numerical methods

To simplify the typography, we introduce the following notation

$$x_1 = V,\ x_2 = [\mathrm{Ca}]_i,\ x_3 = n$$

Defining vector $\mathbf{X}(t) = [x_1(t), x_2(t), x_3(t)]^T$, we can rewrite *Eqs. 1, 12,* and *3* written explicitly for *n* as

$$\frac{d\mathbf{X}}{dt} = F(\mathbf{X}, \mu) \quad (13)$$

where

$$\mathbf{F}(\mathbf{X}, \mu) = [F_1(\mathbf{X}, \mu), F_2(\mathbf{X}, \mu), F_3(\mathbf{X}, \mu)]^T \quad (14)$$

F_1, F_2, and F_3, respectively, stand for the right-hand side of differential *Eqs. 1, 12,* and *3*; μ is the vector of parameters of the model (μ dimension is not specified as alternative models had different numbers of parameters). One-dimensional bifurcations, when parameter I_{dc} was varied, were studied as follows.

Let $\bar{\mathbf{X}}(\mu)$ denotes an hyperbolic equilibrium point of system (*Eq. 13*), i.e., a point satisfying

$$\mathbf{F}[\mathbf{X}(\mu), \mu] = 0 \quad (15)$$

at which location the linearization of vector field $\mathbf{F}[\overline{\mathbf{X}}(\mu)]$ has no eigenvalue with zero real part. Bifurcations of $\overline{\mathbf{X}}(\mu)$ arise when the Jacobean matrix of system *Eq. 13*, $\dfrac{\partial \mathbf{F}}{\partial \mathbf{X}}$, evaluated at $\overline{\mathbf{X}}(\mu)$ is singular

$$\mathbf{det}\left(\frac{\partial \mathbf{F}}{\partial \mathbf{X}}\right)[\overline{\mathbf{X}}(\mu)] = 0 \quad (16)$$

Depending on the value of other parameters, limit cycles emerged at critical I_{dc} values from Hopf or homoclinic bifurcation. Hopf bifurcation arose when a pair of complex eigenvalues of the linearization of vector field $\mathbf{F}[\overline{\mathbf{X}}(\mu)]$ crossed the imaginary axis at nonzero speed. Homoclinic bifurcations were either at saddle-node (the point of coalescence of a stable and an unstable branch in the bifurcation diagram) or at regular saddle (on an unstable branch turning back from a stable branch).

Equation 13 was numerically studied with XPP, Matlab, and Maple V software. Numerical integration in the time-domain was carried out with the stiff-robust method CVODE implemented in XPP. Bifurcation diagrams were built with the AUTO part of XPP. Plateau and valley potentials were quantified to study the particular influence of the different parameters of the model. *Duration* of a plateau (or valley) was defined arbitrarily as the time elapsed between the end of its triggering stimulus and the inflection point in the potential decay at the end of plateaus (valleys); plateaus and valleys of duration <100 ms were discarded because they could not be distinguished by visual inspection from passive exponential relaxation to steady states. *Potential* of a plateau (or valley) was defined as the mean potential within its *duration. Calcium variation* for plateaus and valleys was calculated as the time integral of $[\mathrm{Ca}]_i$ changes from the resting concentration of the cation caused by the stimulus. The plateaus maximum and valleys minimum calcium reached after stimulation were also computed.

RESULTS

Dual electroresponsiveness of the model: plateaus and spikes

Figure 2 illustrates membrane voltage and $[\mathrm{Ca}]_i$ responses of the model to square pulses of depolarizing current that simulated activation of excitatory synapses on the dendrite. Figure 2*A* shows how a large current step ($I_\Phi = 575\ \mathrm{nAcm}^{-2}$) triggered a train of fast Ca spikes, each of them accompanied by a distinct $[\mathrm{Ca}]_i$ transient. The amplitude of the spikes decreased slightly during the first 300 ms of the pulse, but the model settled hereafter into a regular firing mode with a frequency of approximately 10 Hz. The firing abruptly ceased at the pulse offset and *V* recovered to its resting value at −58.3 mV. $[\mathrm{Ca}]_i$ did not fully relax to its resting level between spikes, resulting in a slow increase of the baseline level that culminated at 2.5 μM within 0.3 s after onset of the pulse. Spike-induced $[\mathrm{Ca}]_i$ transients developed with increasing amplitude as the envelope progressively saturated the buffer ($K_d = 1\ \mu$M). Calcium relaxation dynamics were accordingly much slower below 1 μM, compared with higher concentrations; thus $[\mathrm{Ca}]_i$ rapidly fell to 1 μM after the end of the stimulus pulse, but subsequently stayed elevated above its resting level (96 nM) for more than a second after the end of pulse. These features of calcium dynamics correspond very well with optical signals from PCs loaded with Ca-sensitive dyes (see e.g., Lev-Ram et al. 1992; Miakawa et al. 1992; Midtgaard et al. 1993).

The range of voltages sub-threshold to Ca spikes was explored with small amplitude current pulses, which unraveled complex dynamical properties. Figure 2*B* illustrates three samples obtained with 100-ms-duration pulses of different amplitude. With $I_\Phi = 100\ \mathrm{nAcm}^{-2}$, the voltage response was dominated by passive properties of the membrane; *V* decayed exponentially at the end of pulse. This decay was profoundly modified when larger pulses activated nonlinear properties of the membrane. $I_\Phi = 115\ \mathrm{nAcm}^{-2}$ brought the membrane potential to −49 mV, from which *V* recovered to its resting value after a triangular plateau response of 250 ms duration. Increasing I_Φ to $130\ \mathrm{nAcm}^{-2}$ caused a further (approximately 1.5 mV) depolarization at the end of the stimulus. From then on, and instead of repolarizing as before, *V* underwent a slow

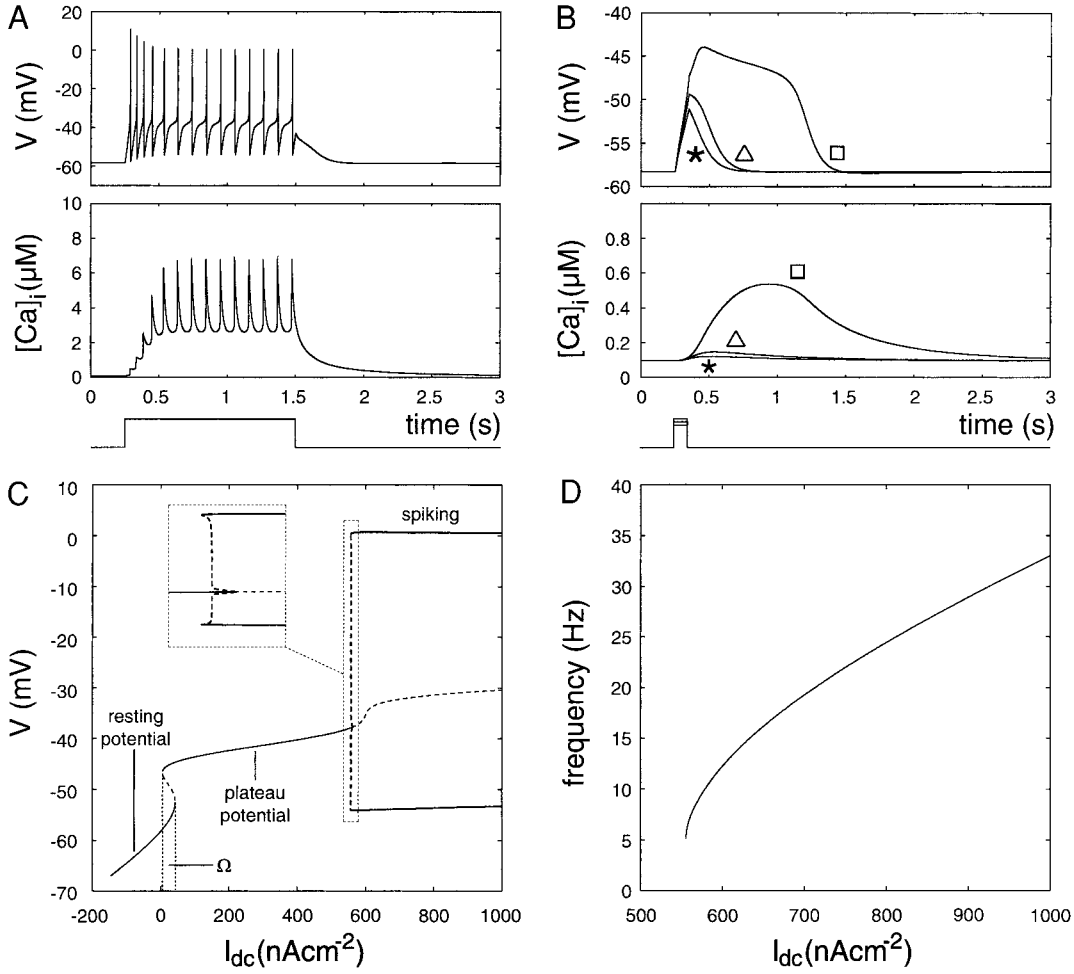

FIG. 2. Spikes and plateaus in the dendritic model. *A*: *V* and $[Ca]_i$ time course during the train of Ca spikes triggered by a long depolarizing pulse ($I_\Phi = 575$ nAcm^{-2}). *B*: sub-threshold responses to brief (100 ms) depolarizing pulses with varied amplitude. The passive response (*), triangular plateau (△), and rectangular plateau (□), respectively, correspond to $I_\Phi = 100$, 115, and 130 nAcm^{-2}. Note the different $[Ca]_i$ scale compared with *A*. *C*: bifurcation diagram obtained by varying I_{dc}. Steady and periodic solutions are respectively depicted as thin and thick lines, stable and unstable solutions as solid and dashed lines. Throughout the text, Ω denotes the current domain where the resting state coexists with an excited, plateau state. *D*: Ca spikes frequency/I_{dc} curve reveals low frequency of discharge.

upward deflection to −45 mV, from which it produced a rectangular plateau of approximately 800 ms duration. *V* slowly drifted toward more negative values during the plateau, and below −49 mV, the model abruptly repolarized with kinetics similar to the triangular plateau. Close resemblance of this repolarizing phase between the two pulses as well as high sensitivity of the response to small current changes implied a voltage threshold in both the triggering and the spontaneous reset of plateaus.

Figure 2*B* (*bottom*) displays the time course of $[Ca]_i$ during the above-mentioned voltage responses. $[Ca]_i$ did not increase significantly from its resting value during the passive response. A very limited increase (peak approximately 150 nM) accompanied the triangular plateau, which can be related to the virtual absence of significant $[Ca]_i$ changes reported during short-duration, triangular plateaus (Miyakawa et al. 1992). On the contrary, $[Ca]_i$ increased up to five times its resting value during the rectangular plateau. This result corresponds well with data from Callaway et al. (1995; see Fig. 10) that show marked $[Ca]_i$ increases during long duration, rectangular plateaus.

Faced with such different responses, we investigated the range of possible behaviors of the model by means of the bifurcation theory. Figure 2*C* illustrates the bifurcation diagram obtained by varying the intensity of a tonic current delivered to the model. From *left* to *right*, one first encounters a I_{dc} range where the resting state is a globally stable attractor (*bottomsolid branch*). Just above the zero current axis, a narrow current region is found, where this state coexists with another stable, depolarized state (*topsolid branch*). In this region of hysteresis, the resting state is separated from the excited one by an unstable (dashed) branch. We found that the hysteresis region laid in the range $\Omega = [5.85,42.76]$ of tonic inputs (nAcm^{-2}). With larger currents, the excited state branch exchanged stability at 561.3 nAcm^{-2}, where a limit cycle appeared. Classical algebraic criteria allowed us to show that this limit cycle arose from a Hopf bifurcation (see Mattheij and Molenaar 1996). The new oscillatory branch was unstable and became stable at a turning point (555.6 nAcm^{-2}), demonstrating the subcritical nature of the bifurcation. Thus stable oscillations of the membrane potential started with finite amplitude and corresponded to the regular firing of fast Ca spikes illus-

trated in Fig. 2*A*. The slope of the limit cycle frequency/I_{dc} curve decreased rapidly with increasing currents (Fig. 2*D*), and the relation became close to linear above 700 nAcm^{-2}. I_{dc} = 10^3 nAcm^{-2}, that is about twice the bifurcation current, led only to a 35-Hz frequency, indicating that the model predicted low frequency firing. Compilation of published traces of Ca spike discharge in intracellular recording gives a frequency range of approximately 5–30 Hz (see e.g., Llinas and Sugimori 1980b), which corresponds well with this result.

The Ω range computed above corresponded to a current domain where the model exhibited bistability. However, the bifurcation parameter in Fig. 2*C* was I_{dc}. With $I_{dc} = 0$, phasic inputs failed to switch the membrane to the excited state (Fig. 2*B*). This proved that the origin of the spontaneous reset of plateaus was not to be found in the bistability of the model. The following section investigates the mechanism of this reset.

Mechanism of spontaneously resetting plateaus

The ionic basis of spontaneously resetting plateaus (Fig. 2*B*) was difficult to determine from the full equation system, owing to its three-dimensionality. We therefore attempted to simplify this system. It was tempting to remove g_{Kdr} from the model, because this conductance never activated more than 5% of its maximum value during plateaus. However, in the range [−50, −40] mV, g_{Kdr} and g_{Ksub} were of the same order of magnitude, suggesting that plateau generation involved the two K conductances. This was confirmed by zeroing either of the two K conductances (Fig. 3). With g_{Ksub} suppressed (g_{Kdr} left unchanged), the model lost its capacity to sustain plateaus; but it could still fire Ca spikes, showing that spikes arose from interaction between I_{Ca} and I_{Kdr}. When g_{Kdr} was suppressed (g_{Ksub} left unchanged), the model lost its ability to sustain either Ca spikes or sub-threshold plateaus. Instead, current pulses switched the membrane to a highly depolarized stable potential (approximately 52 mV). This result reproduced the large plateau at 55 mV observed by Llinas and Sugimori (1980a) after blocking K conductances with tetraethylammonium remarkably well.

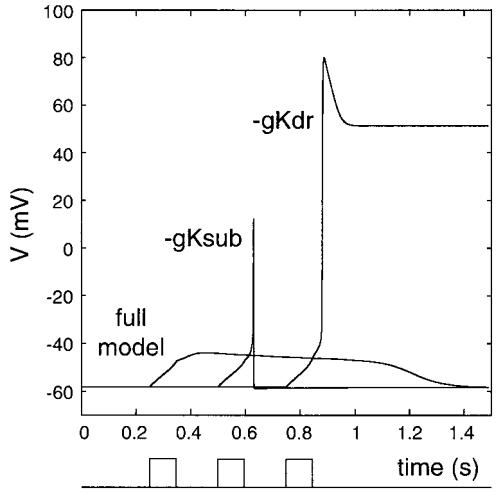

FIG. 3. Mixed activation of I_{Ksub} and I_{Kdr} during finite-duration plateaus. A 100-ms pulse (I_Φ = 130 nAcm^{-2}) was used to trigger a plateau with spontaneous reset in the full model. The same pulse triggers a Ca spike in the model devoid of g_{Ksub}. Without g_{Kdr}, the pulse switches the model to a stable plateau state at a highly depolarized level (onset of the 3 pulses was shifted for clarity of the graph).

The above results show that the three active currents interacted strongly during plateaus. Nevertheless, the n variable evolved on a much faster time-scale than V and $[Ca]_i$ during plateaus. This suggested that plateaus could be studied by considering the slow sub-system formed by the two latter variables. We therefore set $n = n_\infty(V)$ in the full system to obtain a degenerate system with V and $[Ca]_i$ as variables. Figure 4*A* plots trajectories of the variables of this two-dimensional model in response to a 100-ms depolarizing pulse (I_Φ = 130 nAcm^{-2}). The V and $[Ca]_i$ traces closely matched those illustrated for the full model with the same pulse in Fig. 2*B*. Figure 4*B* displays the instantaneous *I/V* relation of the reduced model (i.e., at fixed $[Ca]_i$) at three different times, before and during the plateau, marked by vertical dashed lines in Fig. 4*A*. Intersections of these curves with the V axis were not true equilibria of the reduced model, but equilibria of the V differential equation for given instantaneous values of $[Ca]_i$. As such, location of V-equilibria along the V axis evolved in time with $[Ca]_i$ changes. Three V-equilibria were found prior to the stimulus (Fig. 4*B*, curve labeled with an asterisk). The left (approximately −58.3 mV) and right ones (−42.1 mV) were stable (●) and corresponded, respectively, to the resting state and to an excited state of the model. The middle equilibrium point (○) was unstable (stability can be assessed from the sign of the local slope of the *I/V*). Figure 4*A* plots the time evolution of the voltage of the unstable and excited V-equilibria, superimposed on the membrane voltage trace. The current pulse depolarized the membrane beyond the unstable equilibrium and the model switched toward the excited state. However, due to the slow $[Ca]_i$ increase occurring during the early part of the plateau, the driving force of I_{Ca} diminished progressively, resulting in a slow upward shift of the *I/V* (Fig. 4*B*). This shift forced the unstable and excited states to approach each other until they coalesced (Fig. 4*B*, ×) at the instant marked by a triangle in Fig. 4*A*. The model was then forced to recover its resting state, as it was the only equilibrium point left. Full recovery of the resting state was granted by the fact that, as $[Ca]_i$ rediminished, the excited and unstable states reappeared only after V had decayed under the unstable V-equilibrium.

As the reduced model was two-dimensional, the above features were best captured in the ($[Ca]_i$, V) plane. Figure 4*C* illustrates two significant trajectories of the reduced model in this plane and depicts the nullclines. A 100-nAcm^{-2} pulse resulted in a 8-mV transient depolarization, accompanied by a moderate $[Ca]_i$ increase (peak approximately 150 nM). With I_Φ = 130 nAcm^{-2}, membrane voltage was made to cross the V-nullcline, which it did nearly horizontally owing to the slow rate of $[Ca]_i$ evolution. From then on, the trajectory turned leftward to follow the right-most branch of the V-nullcline. In this region, the overall dynamics of the model were governed by the slow $[Ca]_i$ dynamics; this part of the trajectory corresponded to the plateau part of the response. The trajectory eventually went beyond the local maximum of the V-nullcline, crossed the $[Ca]_i$ nullcline, and finally returned to the resting state; this last phase of the trajectory corresponded to the rapid plateau decay.

Figure 4*D* quantifies properties of spontaneously resetting plateaus as a function of I_Φ (100-ms-duration pulses). Nonlinear membrane properties began to activate at 110 nAcm^{-2} and led to the triangular plateaus illustrated in Fig. 2*B*. Their mean

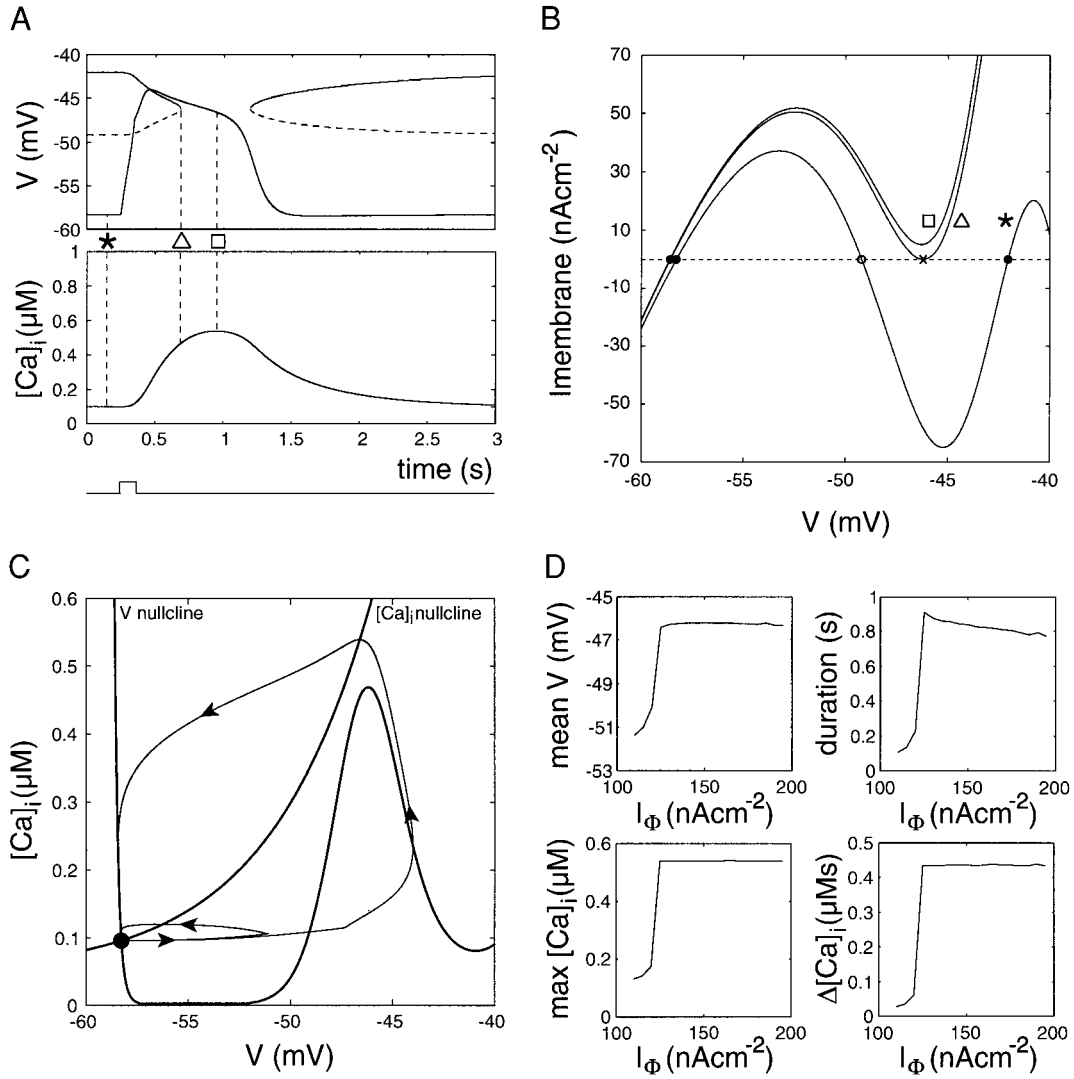

FIG. 4. Mechanism of spontaneously resetting plateaus in the model with $I_{dc} = 0$. Graphs illustrate the dynamics of the 2-dimensional system derived from the model by assuming instantaneous activation of I_{Kdr}. *A*: time course of V and $[Ca]_i$ in response to a 100-ms depolarizing pulse ($I_\Phi = 130$ nAcm^{-2}); traces faithfully reproduce those obtained with the full model with the same stimulation (Fig. 2*C*). *B*: instantaneous dendritic *I/V* relation at the 3 times marked by dashed vertical lines in *A*. Before the pulse (*), the *I/V* intersects the 0-current axis at 3 points, which represent pseudo-equilibrium voltages (or *V*-equilibrium) (●, stable; ○, unstable). Voltages of the middle (dashed) and right (solid) *V*-equilibrium are superimposed on the *V* trace in *A*. Depolarization above the middle (saddle) point brings the system toward the right (plateau) equilibrium. As $[Ca]_i$ increases, I_{Ca} decreases, which shifts the *I/V* relation upward. This brings the 2 right equilibrium points closer, until they coalesce (△), and V is then forced to return to its resting value. Note that, after reaching a maximum (□), $[Ca]_i$ decreases and allows the saddle and plateau points to reappear; but V has already decayed under the saddle voltage at this time and the dendrite keeps repolarizing. *C*: phase plane analysis. Trajectory of the plateau illustrated in *A* (outer trajectory) and a passive response (inner trajectory) to a smaller, 100-nAcm^{-2} pulse are displayed in the (V, $[Ca]_i$) plane. Graph also displays the $[Ca]_i$-nullcline ($d[Ca]_i/dt = 0$) and V-nullcline ($dV/dt = 0$), which intersect at a stable state (solid dot) corresponding to the resting potential. From this point, a trajectory must be driven by an injected current across the unstable middle branch of the V-nullcline to form a rectangular plateau. *D*: quantitative analysis of resetting plateaus as a function of I_Φ (100-ms-duration pulse). Steep region on the left of curves corresponds to triangular plateaus, while the flat part corresponds to rectangular plateaus.

potential, duration, $[Ca]_i$ peak, and $[Ca]_i$ deviation all increased steeply up to $I_\Phi = 125$ nAcm^{-2}. Beyond this value, plateau potentials became largely insensitive to I_Φ and adopted a stereotyped rectangular form. Thus rectangular plateaus were characterized by a uniform amplitude (approximately −46 mV) and duration (~800 ms), which translated into nearly constant $[Ca]_i$ peak (~550 nM) and deviation (~450 nMs).

According to the above analysis, spontaneously resetting plateaus reflected the excitability of the resting state of the model. Looking at Fig. 4*C*, one recognizes an homology between geometrical properties of this point and that of the resting state in Fitzhugh-Nagumo's model (in the parameter range where it has an excitable resting state, see Murray 1993). This analogy suggests that finite-duration plateaus triggered by phasic currents represent genuine action potentials, with a much slower time course and lower amplitude than fast Ca spikes. However, these spike-like plateaus were obtained without tonic currents. In our model, I_{dc} was able to shift the operating regime of the dendrite in response to phasic inputs with respect to the hysteresis region (Fig. 2*C*). We therefore

investigated model properties at different levels of depolarizing tonic currents.

Stable plateaus

Figure 5 illustrates how feeding the model with $I_{dc} = 25$ nAcm^{-2} (laying at the center of Ω) modified responses to phasic inputs. A 35-nAcm^{-2}, 100-ms duration pulse triggered a transient depolarization that decayed passively after the pulse. But $I_{\Phi} = 100$ nAcm^{-2} switched the dendrite to -45 mV, this excited state being maintained indefinitely after the pulse. The transient 4-mV hyperpolarization triggered by a -35-nAcm^{-2} negative pulse, delivered at time $t = 1.5$ s, demonstrates the stability of this plateau. However, the model could be switched back to its unexcited state by a -100-nAcm^{-2} pulse.

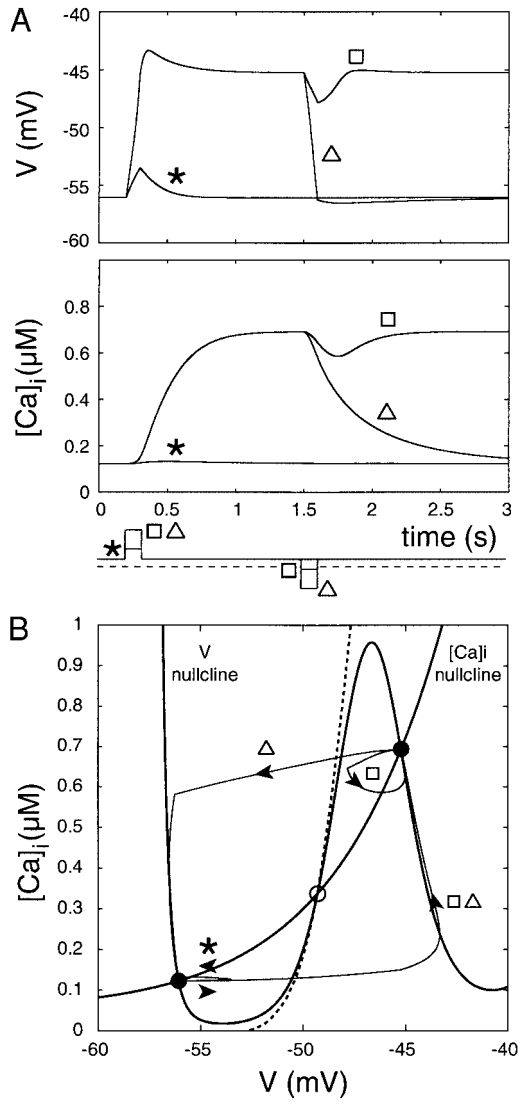

FIG. 5. Stable plateau in the reduced model with $I_{dc} = 25$ nAcm^{-2}. *A*: V and $[Ca]_i$ responses to brief (100 ms) depolarizing pulses. With $I_{\Phi} = 35$ nAcm^{-2} (*), the model returns to its resting state, while $I_{\Phi} = 100$ nAcm^{-2} (△, □) switches the model to a plateau state. Stability of the plateau is illustrated by the transient hyperpolarization triggered by a small hyperpolarizing pulse (□, $I_{\Phi} = -35$ nAcm^{-2}). The dendrite can be, however, switched off to its resting state by a larger pulse (△, $I_{\Phi} = -100$ nAcm^{-2}). *B*: phase plane representation reveals the origin of this threshold behavior. *Traces* shown in *A* (thin lines) are displayed in the (V, $[Ca]_i$) plane, together with the V- and $[Ca]_i$-nullclines of the system (thick traces). Reduced model has 2 stable attractors (resting and plateau states, ●) and an unstable equilibrium (saddle, ○). Starting from 1 of the 2 stable points, a trajectory must cross the stable manifold of the saddle (dashed line) to converge to the other stable point.

The origin of these features is more evident in Fig. 5*B*, which illustrates how the tonic input modified nullclines of the reduced two-dimensional model. I_{dc} had shifted the V-nullcline upward, resulting in a saddle-node bifurcation. This led to the appearance of two additional equilibrium points in contrast with the zero tonic input diagram (Fig. 4*C*). The right most equilibrium corresponded to a plateau state of the membrane and was stable, like the resting state. The central point was a saddle, whose stable manifold separated the basins of attraction of the resting and plateau states and therefore acted as a threshold between the two stable states (dashed curve in Fig. 5*B*). Thus perturbations of the resting state that stayed to the left of the stable manifold eventually died away; perturbations of the plateau state that stayed to the right of the stable manifold also died away. But any perturbation from one of the stable states, large enough to cross the stable manifold, brought the model over to the other state. In these conditions, the dendrite behaved like a switch between the resting and plateau states, as was suggested by Yuen et al. (1995). However, the model of these authors predicted very depolarized potentials for stable plateaus (~0 mV), whereas the ones obtained in our reduced (Fig. 5*A*) and full models (Fig. 2*C*) were clearly sub-threshold, consistent with experimental observations (Llinas and Sugimori 1980b).

Valley potentials

A third kind of dynamical behavior was obtained with I_{dc} larger than the upper bound of the Ω range. With such tonic inputs, the model had a globally stable attractor, corresponding to a stable plateau state. Whatever initial conditions, the dendrite eventually converged to this state because the lower stable branch in the bifurcation diagram had vanished. Thus short inhibitory inputs could not switch off the dendrite to a de-excited state as they did previously. Figure 6*A* shows, however, that the plateau exhibited complex dynamical responses to such brief inputs. Thus a -50-nAcm^{-2}, 100-ms duration pulse resulted in a transient passive hyperpolarization. Increasing the intensity to -75 nAcm^{-2} turned this passive response into a triangular, inverted plateau of approximately 150 ms duration. Further increase of I_{Φ} to -100 nAcm^{-2} lengthened this response to 1 s. Comparison with Fig. 2*B* shows how the time course of V and $[Ca]_i$ during these responses mirrored dynamics of the variables during spontaneously resetting plateaus. These inverted plateaus were therefore termed "valley potentials." The shape of rectangular valleys was robust to increases in I_{Φ} as can be seen from the trace with the -150-nAcm^{-2} pulse. This shows that the model could produce a stereotyped trace of past inhibitory inputs. However, Fig. 6*A* suggests that such traces could take place only following inhibitory inputs with a magnitude sufficient to bring V under a threshold located around -50 mV. This threshold behavior can be understood in Fig. 6*B*, which plots trajectories of the reduced model in the ($[Ca]_i$, V) plane. The resting and saddle points had coalesced, leaving the plateau as the unique steady state. As V evolved faster than $[Ca]_i$, the vector field was nearly horizontal in the portion of the plane considered, except near branches of the

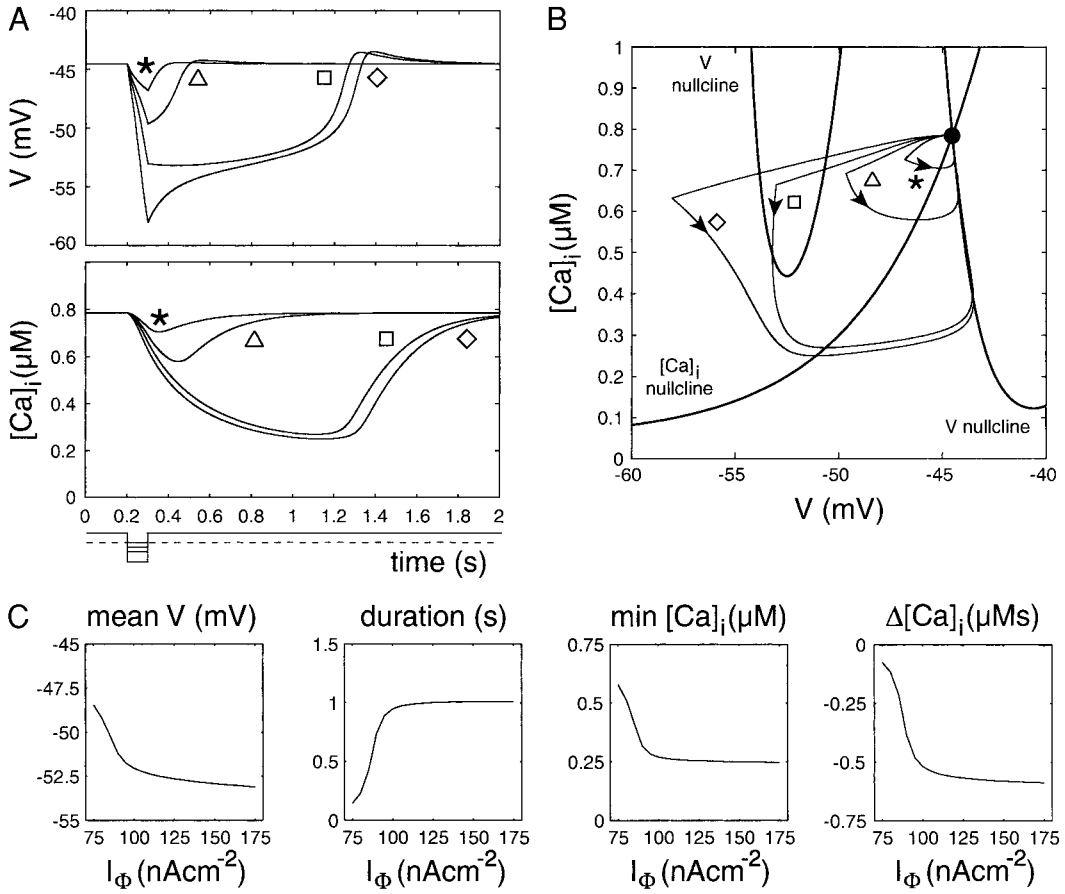

FIG. 6. Valley potentials in the reduced model with $I_{dc} = 50$ nAcm^{-2}. *A*: responses to 100-ms hyperpolarizing pulses from the stable plateau potential (I_Φ = *, −50; △, −75; □, −100; and ◇, −150 nAcm^{-2}, see *bottom traces*). Mirroring plateaus (compare to Fig. 2*A*), increasing magnitude of hyperpolarizing pulses turn a passive response into triangular and rectangular responses. *B*: representation in the phase plane illustrates changes in the nullclines intersections. Single equilibrium point left corresponds to the plateau state (●). This point is excitable, and trajectories that cross the middle branch of the *V*-nullcline form rectangular valleys (■ and ◇). *C*: quantitative analysis of resetting valley potentials as a function of I_Φ.

V-nullcline, where the field was tilted vertically. This implicates that model dynamics were controlled by the $[Ca]_i$ differential equation in these regions. Thus with growing pulse amplitude, perturbations approached the U-shaped region of the *V*-nullcline where their relaxation was slowed down by $[Ca]_i$ dynamics (i.e., triangular valleys). Perturbations that were just large enough to cross the middle branch of the V-nullcline induced rectangular valleys; the slow phase of these valleys corresponded to the part of the trajectory that ran along the middle branch of the *V*-nullcline. With larger pulses, perturbations could even cross the left branch of the *V*-nullcline. These trajectories were quickly brought back toward the U-shaped region of the *V*-nullcline, thereby producing a peak hyperpolarization followed by a stereotyped valley potential.

Figure 6*C* summarizes characteristics of valley potentials as a function of I_Φ. From 75 to 90 nAcm^{-2}, phasic inputs triggered triangular valleys at more hyperpolarized levels and with growing duration. The minimum $[Ca]_i$ reached and integrated $[Ca]_i$ diminution continuously decreased with increasing hyperpolarizing phasic inputs. $I_\Phi = 90$ nAcm^{-2} represented a threshold value, above which rectangular valley potentials adopted stereotyped characteristics (mean level approximately −53 mV, 1 s duration; $[Ca]_i$ peak at 250 nM and $[Ca]_i$ deviation of 0.5 μMs).

Global behavior

The previous sections have shown that the plateaus with spontaneous reset, which could be triggered by a brief depolarizing pulse (Figs. 1 and 3), were transformed into infinite-duration plateaus by injecting a tonic current laying in the Ω range (Fig. 5). It is apparent from this result that I_{dc} was able to modulate the length of plateaus in the model. This property of tonic currents was analyzed in details. In Fig. 7*A*, on the left of the Ω region, are displayed four examples of curves relating the duration of a plateau triggered by a depolarizing pulse to the magnitude of the applied I_{dc}. The pulse duration was 100 ms in all cases, and I_Φ had the following amplitudes (nAcm^{-2}): 150 (×), 200 (+), 250 (◇), and 300 (□). Figure 7*A* shows that hyperpolarizing tonic currents prevented the pulses from triggering plateau potentials, down to a critical I_{dc} value where plateaus emerged with a triangular shape. This critical current value was more negative when I_Φ was large, ranging from about −100 nAcm^{-2} for $I_\Phi = 300$ nAcm^{-2} to −25 nAcm^{-2} for $I_\Phi = 150$ nAcm^{-2}. Whatever the value of I_Φ, reducing the magnitude of the tonic hyperpolarizing current from the critical value increased sharply the duration of triangular plateaus, up to a point where plateaus adopted a rectangular shape; this change of shape occurred at the I_{dc} values where the curves

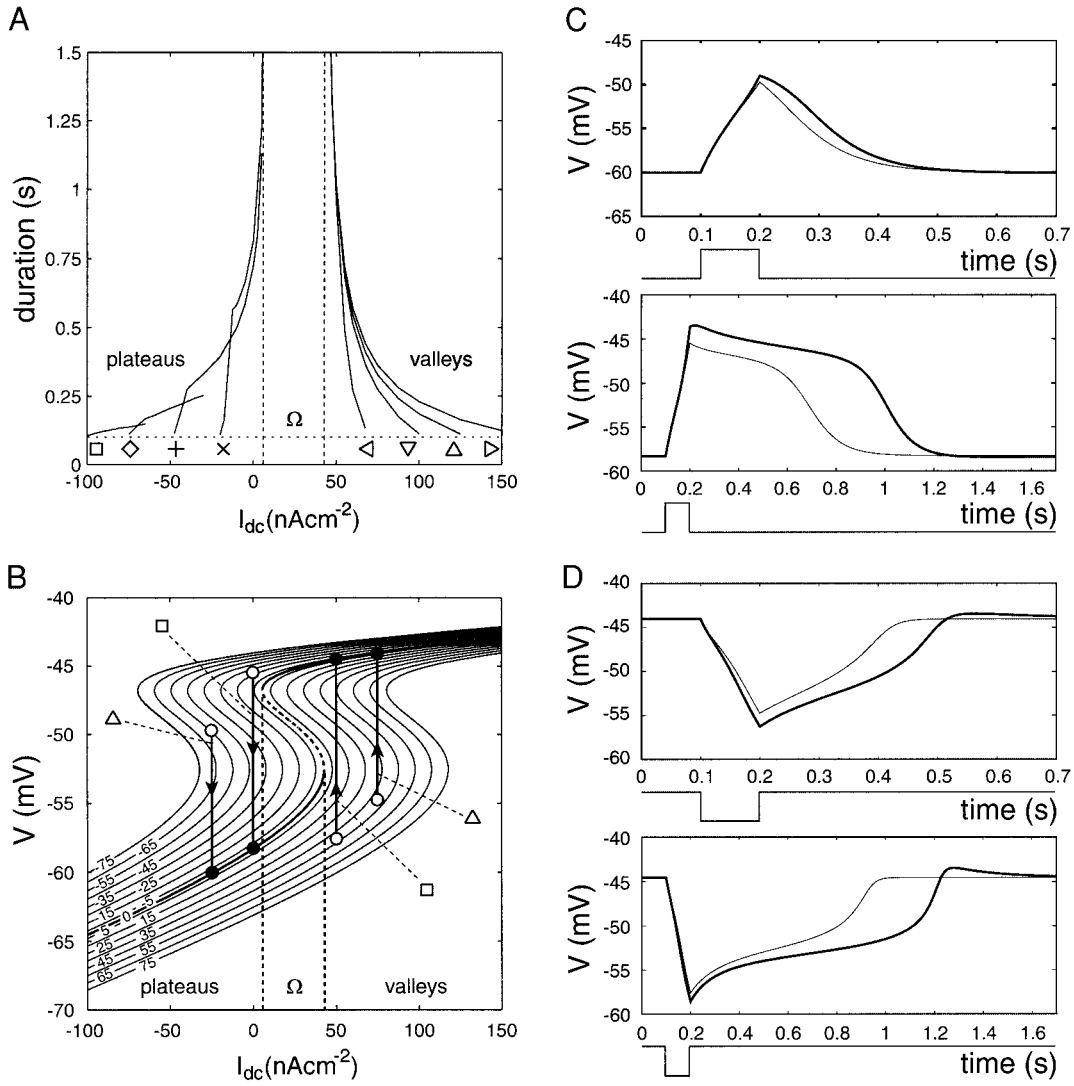

FIG. 7. Global behavior of the model. *A*: duration of plateaus and valleys as a function of I_{dc}. Plateaus and valleys were triggered by 100-ms pulses with the following I_Φ value (nAcm^{-2}). Plateaus: 300 (□), 250 (◇), 200 (+), 150 (×); valleys: –100 (◁), −150 (▽), −200 (△), −300 (▷). *B–D*: origin of the influence of I_{dc} on the duration of sub-threshold responses. By assuming that $[Ca]_i$ and *n* are at equilibrium at each point in time, the full model was reduced to a 1-dimensional model with variable *V*. *B*: subset of constant *dV/dt* curves of the 1-dimensional model in the (I_{dc}, *V*) plane; the value of the potential derivative (mVs^{-1}) is indicated by a label on each curve. *C* and *D*: compare the time course of typical sub-threshold responses in the full model (thick lines) and in the 1-dimensional model (thin lines): triangular plateau (*C, top*, $I_{dc} = -25$ and $I_\Phi = 155$), rectangular plateau (*C, bottom*, $I_{dc} = 0$ and $I_\Phi = 155$), triangular valley (*D, top*, $I_{dc} = 75$ and $I_\Phi = -155$), and rectangular valley (*D, bottom*, $I_{dc} = 50$ and $I_\Phi = -155$). All currents are in nAcm^{-2}, and the pulse duration was 100 ms in each case. Vertical lines in *B* display the corresponding trajectories of the 1-dimensional model in the (I_{dc}, *V*) plane. Arrows indicate the direction of repolarization toward the steady state (resting state for plateaus and plateau state for valleys). Graphs evidence how sequence of slow/fast/slow values of the voltage-time derivative can account for the shape of plateaus and valleys.

exhibit a slope discontinuity. The curves for the 250 and 300 nAcm^{-2} had to be interrupted at $I_{dc} = -30$ and -70 nAcm^{-2}, respectively, because the pulses triggered Ca spikes with hyperpolarizing I_{dc} below these values. The curves for the two smaller pulses could be extended up to the lower bound of the Ω region, where the plateau duration became infinite. Overall, Fig. 7*A* shows that the duration of plateaus in the model could be made to cover an infinite range by varying I_{dc} between approximately -100 nAcm^{-2} and the lower bound of Ω. Experimental plateaus have been reported to range from close to zero duration plateaus (nearly passive responses) to plateaus lasting for several seconds (Ekerot and Oscarsson 1981; Llinas and Sugimori 1992). These latter, long-lasting plateaus may reflect the reset of otherwise stable plateaus by the spontaneous activation of inhibitory synapses; however, no experimental evidence of our knowledge can support or refute this interpretation at the current time. Interestingly, the onset of Ca spikes from plateau potentials predicted from Fig. 7*A* as the phasic input magnitude increases is clearly evident in the voltage traces illustrated by Llinas and Sugimori (1992).

Figure 7*A* also illustrates the influence of I_{dc} on the duration of valley potentials on the right of the Ω region. The 100-ms pulses used to generate these valley duration/I_{dc} curves had the following magnitudes (nAcm^{-2}): –100 (◁), −150 (▽), −200 (△), and −300 (▷). The valley duration decreased as I_{dc} increased, and valleys with the longest duration were found

near Ω like the longest plateaus. In contrast to plateaus, the duration of valleys varied smoothly with I_{dc}. In summary, pulses with an appropriate magnitude could trigger plateaus and valleys within a range of I_{dc} values spanning almost seven times the width of the Ω region.

Figure 7*A* shows, through variations in I_{dc}, that the shape of plateaus and valleys was sensitive to the membrane potential. We devised a qualitative understanding of this influence from a geometrical representation of the model dynamics similar to the method of isoclines (see, e.g., Mattheij and Molenaar 1996). This approach consisted of generating a one-dimensional approximation of the full model by extending to the $[Ca]_i$ variable the rapid equilibrium approximation made for the *n* variable (notice that zeroing the time derivative in *Eq. 12* leaves an algebraic equation that cannot be solved explicitly for $[Ca]_i$ in terms of *V*; strictly speaking, the one-dimensional model was actually a differential algebraic system of equations). Stimulation parameters were adjusted for the full model to produce typical sub-threshold responses (thick curves in Fig. 7, *C* and *D*): a triangular plateau (*C,top*), a rectangular plateau (*C, bottom*), a rectangular valley (*D,top*), and a triangular valley (*D, bottom*). Trajectories were also computed for the one-dimensional model with the same stimulus parameters and are illustrated as thin curves in Fig. 7, *C* and *D*. These trajectories are also represented in the (I_{dc}, *V*) plane as vertical bars in Fig. 7*B*, together with a subset of constant potential derivative curves of the one-dimensional model. Each of these curves indicates the locus of points in the (I_{dc}, *V*) plane where the derivative of state variable, *V*, of the one-dimensional model has a given value (see labels).

The one-dimensional model reproduced qualitatively the shape of either triangular or rectangular plateaus and valleys in the full model. The only difference between the two models was that all active sub-threshold responses had a shorter duration in the one-dimensional model than in the full one, due to the neglecting of slow $[Ca]_i$ dynamics. This result proved that the one-dimensional model could be used to understand the qualitative dynamics of plateaus and valleys.

In a passive model, potential derivative would be straight lines, but in the one-dimensional model these curves were S-shaped due to the activation of I_{Ca} and I_{Ksub} (Fig. 7*B*). Due to this distortion of the potential derivative curves, the one-dimensional model crossed regions of different *dV/dt* values in the (I_{dc}, *V*) plane during the responses illustrated in Fig. 7, *C* and *D*. With the triangular plateau (Fig. 7*C, top*), the membrane potential of the one-dimensional model was −49.7 mV at the end of the pulse. At this voltage, *dV/dt* was $-55\ mVs^{-1}$ (Fig. 7*B*) and this relatively low *dV/dt* value entailed the initial slow rate of repolarization of the one-dimensional model (Fig. 7*C*). As the plateau decayed, however, the rate of repolarization accelerated because the model crossed regions with growing values of *dV/dt* until it approached its resting state. Then, the model encountered again a region with low *dV/dt* value, which was responsible for the slow phase terminating the triangular plateau in the one-dimensional model (Fig. 7*C*). The rectangular plateau on the *bottom* of Fig. 7*C* had a longer duration because, at the value of $I_{dc} = 0$, the trajectory of the one-dimensional model intersected constant potential derivative curves with globally smaller *dV/dt* values than with the triangular plateau. Thus the smallest *dV/dt* value met during the rectangular plateau was $-10\ mVs^{-1}$ versus $-50\ mVs^{-1}$ during the triangular plateau. It is seen in Fig. 7*C* how the sequence of slow/fast/slow potential derivatives in the one-dimensional model accounted well for the qualitative shape of plateaus in the full model. Similar conclusions can be derived from Fig. 7, *B* and *D*, as regard to the valley potentials. Thus the simplified one-dimensional model shows that plateaus and valleys stood as a direct consequence of the distortion of the voltage/current relationship around the Ω region, due to the activation of I_{Ca} and I_{Ksub}.

Robustness of results and alternative schemes

The parameter sensitiveness of the results was examined systematically. Particular emphasis was placed on the influence of the parameters on the Ω region, due to its critical role in setting sub-threshold responses of the model. Figure 8, *A* and *B*, shows that increasing g_{Ksub} narrowed Ω by positively shifting the left endpoint of the excited stable branch in the bifurcation diagram. Decreasing g_{Ksub} widened Ω with the opposite effect and also shifted the right endpoint of the excited branch (the Hopf bifurcation) toward the left of the diagram. First, this shift resulted in transition from the Hopf to a homoclinic bifurcation at regular saddle at $g_{Ksub} = 25.25\ \mu Scm^{-2}$ (marked by a vertical dashed line through Ω). With further decrease in g_{Ksub}, the excited branch eventually lost stability at a lower I_{dc} than the right endpoint of the resting branch (Fig. 8*B*), turning Ω into a current domain where the model could still display bistability, but no longer hysteresis. To highlight the difference, Ω boundaries were plotted as dashed lines when Ω corresponded to a bistable region (same symbols were used to locate Hopf/homoclinic and hysteresis/bistability transitions throughout Fig. 8). Note that Ω vanished for $g_{Ksub} = 15\ \mu Scm^{-2}$, due to the coalescence of the left and right endpoints of the excited branch. Figure 7, *C* and *D*, illustrates the effects of changing activation parameters of g_{Ksub}. Ω rapidly vanished when the half-activation potential V_u became more negative, while less negative V_u widened Ω up to $V_u = -37.95$ mV, where Ω vanished. Overall, Fig. 8*C* shows an approximate 10-mV-wide range of V_u values in which the model had a significant region of hysteresis/bistability. As seen in Fig. 8*D*, Ω was widened when g_{Ksub} activated with steeper slopes (i.e., smaller k_u). On the other hand, Ω was continuously narrowed by decreasing $k_u \leq 5$ mV, above which Ω vanished. Together, these results show that dynamical behaviors described in previous sections were robust to significant deviations in the sub-threshold K current parameters, but that an overall steep slope of activation was required for the model to reproduce experimental plateaus.

The effects of changing the density of the two other active conductances are illustrated in Fig. 8, *E* (g_{Ca}) and *F* (g_{Kdr}). A Ω region could be obtained with deviations of the two conductances up to approximately 50% around their reference value. Ω remained a true hysteresis region with all tested values of g_{Kdr}, while it became a bistability region with g_{Ca}'s larger than 800 $\mu S\ cm^{-2}$ due to lower thresholds for spiking at these high Ca conductance values.

The *bottom* of Fig. 8 illustrates the influence of several key parameters of $[Ca]_i$ regulation. All results displayed above were obtained with a radius $R_d = 0.5\ \mu m$, corresponding to the thinnest spiny dendrites (Shelton 1985). Figure 8*G* shows that increasing R_d began by steeply increasing the Ω width, which

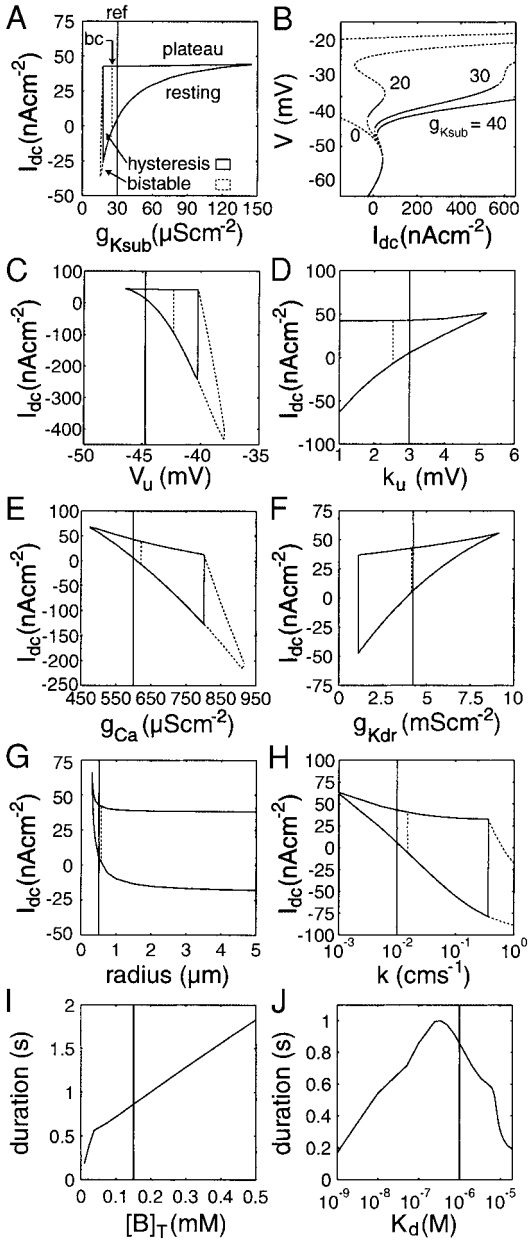

FIG. 8. Sensitivity of the results to parameters. *A* and *C–H*: boundaries of the Ω region, found in the bifurcation diagram in Fig. 2*C*, as a function of different parameters. Influence of parameters on the diagram is illustrated in *B* with the example of g_{Ksub}. For $g_{Ksub} > 20$ μScm^{-2}, a true hysteresis region exists. Below this value, hysteresis is lost, because the plateau branch ends before the resting one, but Ω remains a bistable domain. To display this difference, Ω boundaries are plotted as solid lines with hysteresis and as dashed lines without hysteresis in all graphs. A dashed vertical line across Ω ("bc" in *A*) separates 2 regions in which spikes arise from a Hopf (*right*) or from a homoclinic bifurcation at regular saddle (*left*). Solid vertical line ("ref" in *A*) marks the reference parameter value. *I* and *J*: influence of Ca-buffer parameters (concentration $[B]_T$ and dissociation constant K_d) on the duration of a spontaneously resetting plateau; plateau was triggered by a 100-ms pulse (I_Φ = 130 nAcm^{-2}).

became nearly constant between 1 and 5 μm (corresponding to the primary dendritic trunk). According to our model, all parts of PC dendrites should thus be able to sustain dynamical behaviors described above. Figure 8*H* displays essentially similar results when parameter *k* was varied in a large range around its reference value (*k* sets the time constant that relaxation of $[Ca]_i$ would exhibit without buffer in the cytoplasm). Finally, Fig. 8, *I* and *J*, illustrates the effects of varying the total buffer concentration, $[B]_T$, and its dissociation constant, K_d, on the duration of a spontaneously resetting plateau (triggered by a 130-nAcm^{-2}, 100-ms-duration pulse with $I_{dc} = 0$). With increasing $[B]_T$, triangular plateaus of growing duration were first encountered. $[B]_T = 0.3$ μM marked appearance of rectangular plateaus; their duration increased linearly with the buffer concentration. This feature reflects the ability of the buffer to slow down $[Ca]_i$ dynamics in the range of the cation concentration corresponding to the plateaus. Figure 8*J* shows that K_d's around 0.35 μm resulted in maximal duration plateaus. Decreasing K_d from this value shortened the plateaus because it allowed the buffer to saturate at lower $[Ca]_i$ levels, thereby reducing its efficiency at slowing down $[Ca]_i$ dynamics during plateaus. With K_d's > 0.35 μM, plateaus were also shortened because the buffer slowed down $[Ca]_i$ dynamics at higher $[Ca]_i$ levels than those reached during plateaus.

Additional computations were carried out with I_{ksub} inactivating with time constants ranging from that of the rapid A-current of Wang et al. (1991) to that of the slowly inactivating current hypothesized by Midtgaard (1995). Figure 9*A* displays boundaries of the Ω region in the model with inactivation versus g_{Ksub} (boundaries did not depend on τ_h, which was taken as a constant). The graph is similar to that obtained without inactivation (Fig. 8*A*), except Ω occurred in a g_{Ksub} range above that found in the model without inactivation. This difference stemmed from the voltage dependence of h_∞, which resulted in significant inactivation of g_{Ksub} at rest. Introduction of the inactivation scheme also changed the bifurcation from which the limit cycle emerged into a homoclinic bifurcation at saddle-node in the entire g_{Ksub} range studied. As suggested by the Ω region in Fig. 9*A*, the model with inactivation also produced finite duration plateaus and valleys with appropriate levels of tonic currents (not shown). However, the time constant of inactivation τ_h modulated their duration as illustrated with plateaus in Fig. 9*B*. The figure plots the length of a finite-duration plateau (130-nAcm^{-2}, 100-ms-duration pulse) versus τ_h for three values of g_{Ksub}: 40.66, 75, and 100 μS cm^{-2}. With the value of 40.66, the model had the same density of active sub-threshold K channels at rest as in its basic formulation. With this value, decreasing τ_h continuously increased the plateau duration, which became infinite at $\tau_h = 2$ s; the model discharged a Ca spike below this critical value. Plateaus were lengthened by the decay of I_{ksub} as it partly overcame the decrease in I_{Ca} responsible for the spontaneous resetting of plateaus. This effect was enhanced by decreasing τ_h down to the critical value where I_{ksub} decayed too fast to prevent *V* from reaching the spike threshold. Critical τ_h could be decreased by using larger g_{Ksub} values ($\tau_h = 50$ ms with $g_{Ksub} = 75$ and $\tau_h = 1$ ms with $g_{Ksub} = 100$). With these larger g_{Ksub} values, however, plateau duration decreased in the neighborhood of the critical τ_h instead of becoming infinite. As critical τ_h was approached, this duration decreased due to an early transient depolarization of growing amplitude (data not shown). This resulted in a larger initial $[Ca]_i$ increase at the plateau onset that advanced the resetting effect.

The basic version of the model omitted Ca-dependent K conductances, while it highlighted a critical role for $[Ca]_i$ changes in plateau generation. We therefore introduced a Ca-dependence of I_{ksub} based on Jacquin and Gruol's (1999) data.

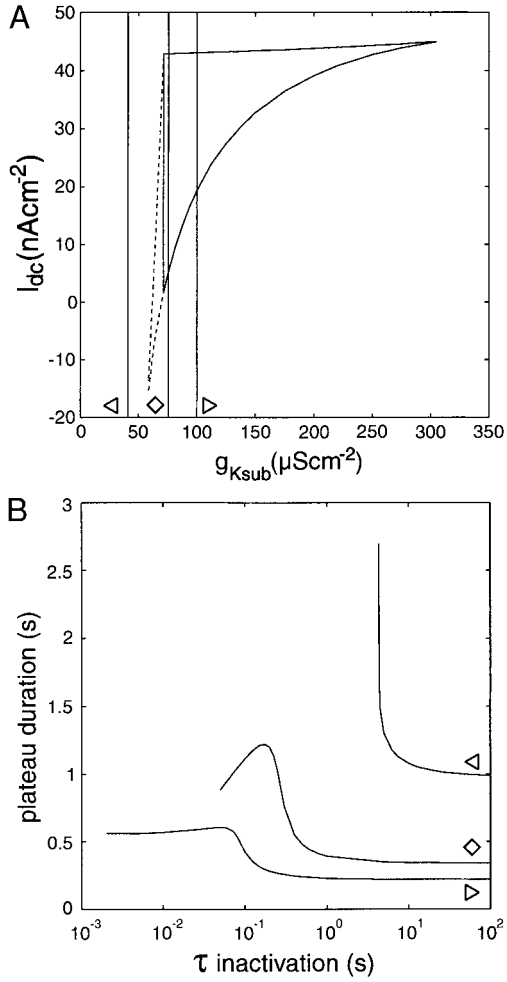

FIG. 9. Model with inactivation of g_{Ksub}. *A*: boundaries of Ω as a function of g_{Ksub}. Dashed triangle on the *left* corresponds to a parameter range, where Ω is a bistable region without true hysteresis. *B*: duration of a spontaneously resetting plateau as a function of the time constant τ_h of inactivation of g_{Ksub}. Plateau triggered by a 100-ms pulse (I_Φ = 130 nAcm^{-2}). Graph displays results obtained with 3 g_{Ksub} values: 40.66 (◁), 75 (◇), and 100 μScm^{-2} (▷). The model discharges Ca spikes with τ_h values below the left endpoint of the curves.

With this modification, the model failed to produce any long-lasting responses to phasic inputs, either plateaus, bistability, or valley potentials (data not shown). Inability of the model to sustain this kind of responses arose because activation of I_{ksub} became controlled by the slow $[Ca]_i$ dynamics. In other words, I_{ksub} activated too slowly in front of I_{Ca} for the two currents to produce the balance required for plateau generation.

DISCUSSION

The model analyzed in this paper accounts for the major features of the dual electroresponsiveness of PC dendrites. It sustains finite-duration plateaus with the various shapes reported in response to parallel fiber volleys (Campbell et al. 1983), activation of the climbing fiber (Ekerot and Oscarsson 1981), or direct electric stimulation (Llinas and Sugimori 1980b, 1992). The model also reproduces the transition from plateaus to spikes with increasing stimulation, as reported by Llinas and Sugimori (1980b, 1992). The robustness of these results relative to large deviations in key parameters around their standard value suggests that our model, despite its low-dimensionality, provides a valuable account of the input-output relation of PC dendrites. As the model predicts occurrence of valley potentials in response to inhibitory inputs during stable depolarized states, which have not been observed yet, we will first discuss consistency of the model in relation to synaptic and membrane intrinsic properties of PCs. We will then discuss the significance of the model regarding computations of PC dendrites.

We cannot exclude that other models may reproduce electroresponsiveness of PC dendrites equally well. However, models that have so far attempted to reproduce the dual electroresponsiveness of PC dendrites contain inconsistencies. In the introduction, we discussed that De Schutter and Bower's (1994) model fails to produce dendritic plateaus with spontaneous reset. Miyasho et al. (2001) recently introduced into this model E- and D-type Ca currents, which inactivate with time constants of several tens of milliseconds. In this model, brief depolarizing currents trigger long after-depolarizations that resemble experimental plateaus. But Miyasho et al.'s model comprises low-threshold Ca conductances with densities of the same order (or even larger) than P-type Ca channels, whereas the latter channels sustain the major part of Ca currents into PC dendrites (Usowicz et al. 1992). In fact, Llinas et al. (1989) have shown that FTX toxin, a selective blocker of P-type channels, abolishes spikes and plateaus, which support the idea that a unique type of Ca current underlies both electric signals. We have found that, to realistically reproduce salient features of experimental plateaus with the sole noninactivating P channel, a minimal model needs to contain two kinds of voltage-activated K channels. The delayed-rectifier introduced into our model was clearly identified in PCs, where it serves to repolarize spikes (Gähwiler and Llano 1989; Gruol et al. 1991). The second channel is more conjectural, because g_{Ksub} lumps together several sub-threshold K channels identified in PCs (Gruol et al. 1991), which are not understood well enough to be modeled individually. Among these conductances, the Purkinje BK-type conductance does not seem critical for plateau generation because endowing g_{Ksub} with a quantitative model of its Ca-dependence (Jacquin and Gruol 1999) completely abolished plateaus. On the other hand, overall properties of the model remained unchanged when g_{Ksub} was endowed with inactivations similar to those exhibited by several PC's sub-threshold K channels (Midtgaard 1995; Wang et al. 1991). Moreover, Yuen et al.'s (1995) model of a PC dendrite, which is devoid of such a sub-threshold K current, produces unrealistic plateaus near 0 mV. Due to its steep slope of activation, the idealized g_{Ksub} endows the model with a strong outward *I/V* rectification near −45 mV when g_{Ca} is zero (data not shown), as can clearly be observed in PCs after blocking their Ca conductances (Genet and Kado 1997). Together, these results suggest that the steep activation of g_{Ksub} represents a key property for the generation of sub-threshold plateaus into PCs. However, it must be noted that in the range [−50, −40] mV, the involvement of I_{Kdr} in balancing I_{Ca} to produce plateaus is quantitatively significant (Fig. 3).

Due to the high levels of Ca-binding proteins in PCs, $[Ca]_i$ dynamics must be largely slowed down in the concentration range corresponding to the K_d of these proteins. Neither K_d nor the concentration of these Ca buffers are currently known with precision. The results illustrated in this paper were, however, computed with a buffer concentration, $[B]_T$, falling at the

center of the range of estimated parvalbumin and calbindin concentrations in PCs (100–210 μM, Fierro and Llano 1996). Moreover, Fig. 8 shows that plateau responses in the model withstood large deviations in K_d and $[B]_T$ values. Slow $[Ca]_i$ increases in the sub-threshold voltage range decreased the Ca Nernst potential, thereby reducing the magnitude of I_{Ca} on a time scale of hundreds of milliseconds. This induced the reset of plateaus in the model by breaking the balance between I_{Ca} and the two K currents. According to our model, the large $[Ca]_i$ transients seen in PCs following their synaptic activation (Miakawa et al. 1992) or direct electric stimulation (Lev-Ram et al. 1992) are therefore responsible for the spontaneous reset of experimental plateaus.

With its set of reference parameters, our model is very close to a transition between Hopf and homoclinic bifurcations for emergence of Ca spiking (Fig. 8). With these two bifurcations, oscillations become stable at a turning point, where they have a finite amplitude of low sensitivity to the I_{dc} magnitude. Spiking emerges at null frequency with the homoclinic bifurcation and only at 5 Hz with the Hopf bifurcation (Fig. 2*D*). This difference would be difficult to observe experimentally, and the model was not designed to faithfully reproduce Ca spiking, which probably involves other conductances than those introduced into the model (see Midtgaard 1995). The precise nature of the bifurcation, therefore, appears meaningless within the context of this study.

Our model assigns distinct roles to phasic and tonic inputs, I_Φ triggering nonlinear responses, whose duration is modulated by I_{dc}. A physiological counterpart for these two kinds of excitatory inputs can be found in actual inputs to PC dendrites. Thus spiny dendrites of PCs are bombarded with several thousands of PFs synapses, whose precise pattern of activation is still unknown. Contextual information in the mossy fiber system without specific correlation may activate PFs asynchronously. According to Rapp et al.'s (1992) simulations, individual fibers probably lose any individual functional meaning in these conditions and provide a tonic depolarizing input to PC dendrites, which can be identified as I_{dc} in our model. In addition to this tonic input, synchronous activation of a subset of PFs during a motor task [see the theory of Marr (1969)] may result in a phasic depolarizing input to the dendritic tree. Ekerot and Oscarsson (1981) were indeed able to trigger plateau potentials by stimulating bundles of PFs. The large number of PFs that must be activated synchronously to trigger plateaus initially led to the conclusion that granule cells do not evoke these prolonged responses under physiological conditions (Campbell et al. 1983). Jaeger and Bower (1994) later proved, however, that granule cells can actually do so via the ascending part of their axon, which runs along PC dendrites and provides more powerful excitatory synapses than PFs (Llinas and Sugimori 1999); according to Cohen and Yarom (1998), granule cell ascending axons provide the main source of excitation to the cerebellar cortex when it is activated via the natural mossy-fiber system. The climbing fiber represents another attractive counterpart for I_Φ, as Ekerot and Oscarsson (1981) have observed that plateau potentials terminate the complex spike in vivo. Interestingly, Ekerot and Kano (1985) showed that activation of stellate cells, which make inhibitory synapses on PC dendrites, abolishes the plateau part of the complex spike and result in the failure of the CF to induce long-term depression (LTD). The CF-induced $[Ca]_i$ signal is believed to constitute the initial stimulus for the LTD of parallel fibers (Daniel et al. 1998; Sakurai 1987), so that the result of Ekerot and Kano (1985) suggests a possible role of plateau potentials in the induction of LTD at PF synapses.

Jaeger and Bower (1994) have observed a gradation of synaptic-evoked plateau responses with the stimulus intensity, whereas Llinas and Sugimori (1980b) obtained all-or-none plateaus by direct electric stimulation. Our model supports the idea that plateau potentials are indeed all-or-none events. This feature could be reconciled with the data of Jaeger and Bower (1994) if plateaus can be triggered independently in different branches of PC dendrites, as suggested by Campbell et al. (1983). Jaeger and Bower's (1994) graded responses would thus reflect summation of individual all-or-none plateaus. If so, plateaus would endow PCs with multistability properties in regard to their input-output relation; computational perspectives of networks comprising such multistable units have been recently illustrated by Barto et al. (1999). This hypothesis on multiple plateaus originating in different dendritic branches could be explored by introducing our local model within a multi-compartmental model of the PC.

An important prediction of our model is that the various plateau shapes reported by Ekerot and Oscarsson (1981) only reflect a part of the PC dendrites operating capabilities. Thus with I_{dc} values inside the hysteresis region Ω, the model can be switched to a stable plateau by brief depolarizing inputs. This feature could explain the quasi-stable plateaus observed by Llinas and Sugimori (1980b), even if a clear evidence for a bistability of PC dendrites with large depolarizing DC input is currently lacking. Brief hyperpolarizing currents with sufficient magnitude can actively reset the plateau by making V cross the unstable branch in the bifurcation diagram (Fig. 2*C*). But it suffices that I_{dc} decreases below the lower Ω bound to recover the resting state automatically; this overcomes limitation of theories of bistable dendrites (Baginskas et al. 1993), into which plateaus can only be reset by activation of inhibitory synapses. Transient inhibitory inputs are unable to reset the plateau with I_{dc} above the upper Ω bound. However, such inputs can trigger long-duration valley potentials at approximately -52.5 mV (Fig. 6), from which the resting state is recovered if I_{dc} falls below the upper Ω bound (see Fig. 2*C*). Valleys have not been observed, but these potentials represent a testable prediction of the model that could be used to experimentally validate the proposed membrane mechanisms underlying plateau potentials.

The present model of PC dendrite provides a modeling framework linking detailed cellular experimental data and large scale computational models of the cerebellum. Thus our model suggests that plateaus and valleys constitute short-term memories of phasic inputs and that the control contextual tonic inputs exert on their duration enlarge the computational properties attributable to PC dendrites. These properties, together with plastic changes at PF synapses, LTD (Daniel et al. 1998), and potentiation (Hansel et al. 2001; Hirano 1991), may contribute to the temporal specificity of cerebellar learning, that has been revealed by the Pavlovian conditioning of eyelid responses (Medina et al. 2000) and adaptation of the vestibulo-ocular reflex.

We thank the two referees for sharp criticisms and clever suggestions.

REFERENCES

BAGINSKAS A, GUTMAN A, AND SVIRKIS G. Bi-stable dendrite in constant electric field: a model analysis. *Neuroscience* 53: 595–603, 1993.

BARTO AG, FAGG AH, AND SITKOFF N. A cerebellar model of timing and prediction in the control of reaching. *Neural Comput* 11: 565–594, 1999.

CALLAWAY JC, LASSER-ROSS N, AND ROSS W. IPSPs strongly inhibit climbing fiber-activated $[Ca^{2+}]_i$ increases in the dendrites of cerebellar Purkinje neurons. *J Neurosci* 15: 2777–2787, 1995.

CAMPBELL NC, EKEROT C-F, HESSLOW G, AND OSCARSSON O. Dendritic plateau potentials evoked in Purkinje cells by parallel fibre volley in the cat. *J Physiol (Lond)* 340: 209–223, 1983.

CHEN C AND THOMPSON RF. Temporal specificity of long-term depression in parallel fiber—Purkinje synapses in rat cerebellar slices. *Learn Memory* 2: 185–198, 1992.

COHEN D AND YAROM Y. Patches of synchronized activity in the cerebellar cortex evoked by mossy-fiber stimulation: questioning the role of parallel fibers. *Proc Natl Acad Sci USA* 95: 15032–15036, 1998.

DANIEL H, LEVENES C, AND CRÉPEL F. Cellular mechanisms of cerebellar LTD. *Trends Neurosci* 21: 401–407, 1998.

DE SCHUTTER E AND BOWER JM. An active model of the cerebellar Purkinje cell. I. Simulation of current clamp in slices. *J Neurophysiol* 71: 375–400, 1994.

ECCLES JC, LLINAS R, AND SASAKI K. The excitatory synaptic action of climbing fibres on the Purkinje cells of the cerebellum. *J Physiol (Lond)* 182: 268–296, 1966.

EKEROT C-F AND KANO M. Long-term depression of parallel fibre synapse following stimulation of climbing fibres. *Brain Res* 342: 357–360, 1985.

EKEROT C-F AND OSCARSSON O. Prolonged depolarization elicited in Purkinje cell dendrites by climbing fibre impulse in the cat. *J Physiol (Lond)* 318: 207–221, 1981.

FIERRO L AND LLANO I. High endogenous calcium buffering in Purkinje cells from rat cerebellar slices. *J Physiol (Lond)* 496: 617–625, 1996.

GÄHWILER B AND LLANO I. Sodium and potassium conductances in somatic membranes of rat Purkinje cells from arganotypic cultures. *J Physiol (Lond)* 417: 105–122, 1989.

GENET S AND KADO RT. Hyperpolarizing current of the Na/K ATPase contributes to the membrane polarization of the Purkinje cell in rat cerebellum. *Pflügers Arch* 434: 559–567, 1997.

GRUOL DL, DIONNE VE, AND YOOL AJ. Multiple voltage-sensitive K^+ channels regulate dendritic excitability in cerebellar Purkinje neurons. *Neurosci Lett* 97: 97–102, 1989.

GRUOL DL, JACQUIN T, AND YOOL AJ. Single channel K^+ currents recorded from the somatic and dendritic regions of cerebellar Purkinje neurons in culture. *J Neurosci* 11: 1002–1015, 1991.

HANSEL C, LINDEN DJ, AND D'ANGELO E. Beyond parallel fiber LTD: the diversity of synaptic and non-synaptic plasticity in the cerebellum. *Nature Neurosci* 4: 467–475, 2001.

HESSLOW G, SVENSSON P, AND IVARSSON M. Learned movements elicited by direct stimulation of cerebellar mossy fiber afferents. *Neuron* 24: 179–185, 1999.

HILLE B. *Ionic Channels of Excitable Membranes.* Sunderland, MA: Sinauer Associates, 1992.

HIRANO T. Depression and potentiation of the synaptic transmission between a granule cell and a Purkinje cell in rat cerebellar culture. *Synapse* 7: 321–323, 1991.

HOUK JC, BUCKINGHAM JT, AND BARTO AG. Models of the cerebellum and motor learning. *Behav Brain Sci* 19: 368–383, 1996.

ITO M. *The Cerebellum and Neural Control.* New York: Raven Press, 1984.

JACQUIN TD AND GRUOL DL. Ca^{2+} regulation of a large conductance K^+ channel in cultured rat cerebellar Purkinje neurons. *J Neurosci* 11: 735–739, 1999.

JAEGER D AND BOWER JM. Prolonged responses in rat cerebellar Purkinje cells following activation of the granule cell layer: an intracellular in vitro and in vivo investigation. *Exp Brain Res* 100: 200–214, 1994.

KANEDA M, WAKAMORI M, ITO C, AND AKAIKE N. Low-threshold calcium current in isolated Purkinje cell bodies of rat cerebellum. *J Neurophysiol* 63: 1046–1051, 1990.

LEV-RAM V, MIYAKAWA H, LASSER-ROSS N, AND ROSS W. Calcium transients in cerebellar Purkinje neurons evoked by intracellular stimulation. *J Neurophysiol* 68: 1167–1177, 1992.

LLINAS R AND SUGIMORI M. Electrophysiological properties of in vitro Purkinje cell somata in mammalian cerebellar slices. *J Physiol (Lond)* 305: 171–195, 1980a.

LLINAS R AND SUGIMORI M. Electrophysiological properties of in vitro Purkinje cell dendrites in mammalian cerebellar slices. *J Physiol (Lond)* 305: 197–213, 1980b.

LLINAS R AND SUGIMORI M. The electrophysiology of the cerebellar Purkinje cell revisited. In: *The Cerebellum Revisited*, edited by Llinas R and Sotelo C. Heidelberg: Springer-Verlag, 1992, p. 167–181.

LLINAS R, SUGIMORI M, LIN J-W, AND CHERKSEY B. Blocking and isolation of a calcium channel from neurons in mammals and cephalopods utilizing a toxin fraction (FTX) from funnel-web spider poison. *Proc Natl Acad Sci USA* 86: 1689–1693, 1989.

MAEDA H, ELLIS-DAVIES GCR, ITO K, MIYASHITA Y, AND KASAI H. Supralinear Ca^{2+} signaling cooperative and mobile Ca^{2+} buffering in Purkinje neurons. *Neuron* 24: 989–1002, 1999.

MARR D. A theory of cerebellar cortex. *J Physiol (Lond)* 202: 437–470, 1969.

MAUK MD, MEDINA JF, NORES WL, AND OHYAMA T. Cerebellar function: coordination, learning or timing? *Curr Biol* 10: R522–R525, 2000.

MATTHEIJ RMM AND MOLENAAR J. *Ordinary Differential Equations in Theory and Practice.* New York: John Wiley, 1996.

MCCORMICK DA AND THOMPSON RF. Cerebellum: essential involvement in the classically conditioned eyelid response. *Science* 223: 296–299, 1984.

MEDINA JF AND MAUK MD. Computer simulation of cerebellar information processing. *Nature Neurosci* 3: 1205–1211, 2000.

MEDINA JF, NORES WL, OHYAMA T, AND MAUK MD. Mechanism of cerebellar learning suggested by eyelid conditioning. *Curr Op Neurobiol* 10: 717–724, 2000.

MIAKAWA H, LEV-RAM V, LASSER-ROSS N, AND ROSS W. Calcium transients evoked by climbing fiber and parallel fiber synaptic inputs in guinea pig cerebellar Purkinje neurons. *J Neurophysiol* 68: 1178–1189, 1992.

MIDTGAARD J. Spatial synaptic integration in Purkinje cell dendrites. *J Physiol (Paris)* 89: 23–32, 1995.

MIDTGAARD J, LASSER-ROSS N, AND ROSS W. Spatial distribution of Ca^{2+} influx in turtle Purkinje cell dendrites in vitro: role of a transient outward current. *J Neurophysiol* 70: 2455–2469, 1993.

MIYASHO T, TAKAGI H, SUZUKI H, WATANABE S, INOUE M, KUDO Y, AND MIYAKAWA H. Low-threshold potassium channels and a low-threshold calcium channel regulate Ca^{2+} firing in the dendrites of cerebellar Purkinje neurons: a modeling study. *Brain Res* 891: 106–115, 2001.

MURRAY JD. *Mathematical Biology.* New York: Springer, 1993.

RAPP M, YAROM Y, AND SEGEV I. The impact of parallel fiber background activity on the cable properties of cerebellar Purkinje cells. *Neural Comput* 4: 518–533, 1992.

REGAN LJ. Voltage-dependent calcium currents in Purkinje cells from rat cerebellar vermis. *J Neurosci* 11: 2259–2269, 1991.

SAKURAI M. Synaptic modification of parallel fibre-Purkinje cell transmission in in vitro guinea-pig cerebellar slices. *J Physiol (Lond)* 394: 463–480, 1987.

SALA F AND HERNANDEZ-CRUZ A. Calcium diffusion modeling in a spherical neuron. Relevance of buffering properties. *Biophys J* 57: 313–324, 1990.

SHELTON DP. Membrane resistivity estimated for the Purkinje neuron by means of a passive computer model. *Neuroscience* 14: 111–131, 1985.

STUART G AND HAÜSSER M. Initiation and spread of sodium action potentials in cerebellar Purkinje cells. *Neuron* 13: 703–712, 1994.

SVENSSON P AND IVARSSON M. Short-lasting conditioned stimulus applied to the middle cerebellar peduncle elicits delayed conditioned eye blink responses in the decerebrate ferret. *Eur J Neurosci* 11: 4333–4340, 1999.

TERASAKI M, SLATER NT, FEIN A, SCHMIDEK A, AND REESE TS. Continuous network of endoplasmic reticulum in cerebellar Purkinje neurons. *Proc Natl Acad Sci USA* 91: 7510–7514, 1994.

THOMPSON RF. Neural mechanisms of *Philo Trans R Soc Lond Ser B* 329: 161–170, 1990.

USOWICZ MM, SUGIMORI M, CHERKSEY B, AND LLINAS R. P-type calcium channels in the somata and dendrites of adult cerebellar Purkinje cells. *Neuron* 9: 1185–1199, 1992.

WANG SS-H, DENK W, AND HAÜSSER M. Coincidence detection in single dendritic spines mediated by calcium release. *Nature Neurosci* 3: 1266–1273, 2000.

WANG YW, STRAHLENDOF JC, AND STRAHLENDORF HK. A transient voltage-dependent outward potassium current in mammalian cerebellar Purkinje cells. *Brain Res* 567: 153–158, 1991.

YUEN GL, HOCKBERGER PE, AND HOUK JC. Bistability in cerebellar Purkinje cell dendrites modeled with high-threshold calcium and delayed-rectifier potassium channels. *Biol Cybern* 73: 375–388, 1995.